BIOCHEMISTRY
including biophysical chemistry & molecular biology

Article

pubs.acs.org/biochemistry

An Extended β7α7 Substrate-Binding Loop Is Essential for Efficient Catalysis by 3-Deoxy-D-*manno*-Octulosonate 8-Phosphate Synthase

Timothy M. Allison,[‡] Richard D. Hutton,[‡] Wanting Jiao,[‡] Benjamin J. Gloyne,[‡] Evan B. Nimmo,[‡] Geoffrey B. Jameson,[†] and Emily J. Parker*[,‡]

[†]The Riddet Institute and The Institute of Fundamental Sciences, Massey University, Palmerston North, New Zealand
[‡]Biomolecular Interaction Centre and Department of Chemistry, University of Canterbury, Christchurch, New Zealand

Supporting Information

ABSTRACT: The enzyme 3-deoxy-D-*manno*-octulosonate 8-phosphate (KDO8P) synthase catalyzes the reaction between phosphoenolpyruvate and arabinose 5-phosphate (A5P) in the first committed step in the biosynthetic pathway for the formation of 3-deoxy-D-*manno*-octulosonate, an important component in the cell wall of Gram-negative bacteria. KDO8P synthase is evolutionarily related to the first enzyme of the shikimate pathway, 3-deoxy-D-*arabino*-heptulosonate 7-phosphate (DAH7P) synthase, which uses erythrose 4-phosphate in place of A5P. The A5P binding site in KDO8P synthase is formed by three long loops that extend from the core catalytic $(\beta/\alpha)_8$ barrel, β2α2, β7α7, and β8α8. The extended β7α7 loop is always present in KDO8P synthase yet is not observed for DAH7P synthase. Modeling of this loop indicated interactions between this loop and the extended β2α2 loop; both loops provide key hydrogen-bonding contacts with A5P. The two absolutely conserved residues on the β7α7 loop (Gln and Ser) were mutated to Ala in both the metal-dependent KDO8P synthase from *Acidithiobacillus ferrooxidans* and the metal-independent KDO8P synthase from *Neisseria meningitidis*. In addition, mutants were constructed for both enzymes with the extended β7α7 loop excised to match the DAH7P synthase architecture. Removal of the loop extension severely hindered efficient catalysis, dramatically increasing the K_m^{A5P} and reducing the k_{cat} for both enzymes. Excision of the complete loop was far more detrimental to catalysis than the double mutations of the two conserved Gln and Ser residues. Therefore, the presence of the entire extended β7α7 loop is important for efficient catalysis by KDO8P synthase, with the loop acting to promote efficient and productive binding of A5P.

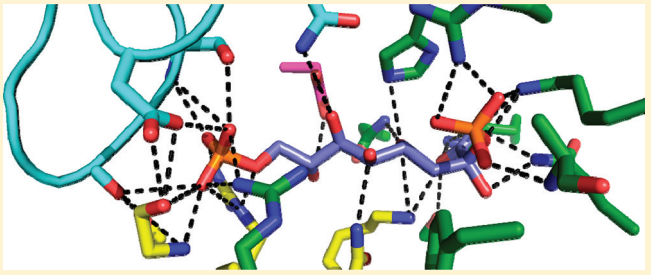

The enzyme 3-deoxy-D-*manno*-octulosonate 8-phosphate (KDO8P) synthase catalyzes the reaction between phosphoenolpyruvate (PEP) and arabinose 5-phosphate (A5P) to form KDO8P. KDO8P is a precursor to 3-deoxy-D-*manno*-octulosonate (KDO), an important component of the lipopolysaccharide layer found in the cell walls of all Gram-negative bacteria.[1] The KDO biosynthetic pathway, and hence KDO8P synthase, is a potential target for antibacterial drug design.[2] KDO8P synthase is mechanistically and evolutionarily related to the first enzyme of the shikimate pathway, 3-deoxy-D-*arabino*-heptulosonate 7-phosphate (DAH7P) synthase.[3−5] DAH7P synthase also uses PEP as a substrate but couples this three-carbon unit with the four-carbon aldehyde erythrose 4-phosphate (Figure 1). It has been proposed that KDO8P synthases evolved from a promiscuous DAH7P synthase-like ancestor.[3,6]

KDO8P synthases and DAH7P synthases share a common $(\beta/\alpha)_8$ TIM-barrel structure.[6−11] The KDO8P synthases and type Iβ DAH7P synthases, the group of DAH7P synthases with which KDO8P synthases share the highest level of sequence identity, adopt similar tetrameric assemblies. Whereas all DAH7P synthases require a divalent metal ion for activity, only some KDO8P synthases retain this metal dependency, while others are proposed to have discarded metal dependency.[3,12] Metal-dependent and metal-independent types of KDO8P synthase can be interconverted;[7,13−17] the primary determinant of metal dependence is the presence at the end of β-strand 1 (β1) of a Cys in the former class and an Asn in the latter.

As with other TIM-barrel enzymes, the active site of KDO8P synthase is found on the C-terminal end of the barrel.[18] The binding of PEP and metal ions is achieved through interactions with residues close to the ends of the β-sheets of the core barrel. PEP and the metal ion binding sites are constructed very similarly in both KDO8P synthases and DAH7P synthases,[6,8,18] and the residues involved are conserved between the two enzymes, with the exception of the Cys to Asn substitution associated with metal dependency. The binding site for A5P protrudes farther from the core of the barrel. Three long loops (β2α2, β7α7, and β8α8), which link the ends of the eponymous β-sheets and corresponding helices, extend from the barrel,

Received: August 7, 2011
Revised: September 23, 2011
Published: September 26, 2011

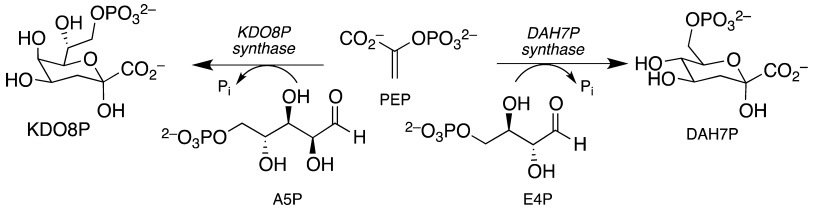

Figure 1. Reactions catalyzed by KDO8P synthase and DAH7P synthase.

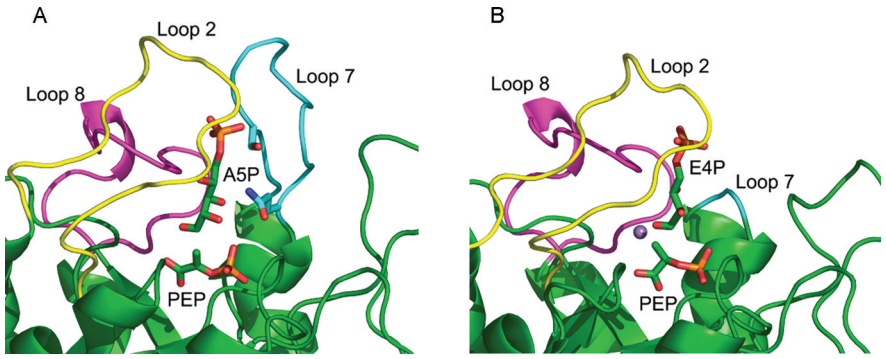

Figure 2. Structures of KDO8P synthase and DAH7P synthase showing the loops that extend from the core barrel and contribute to the active-site architecture. (A) *Aae*KDO8PS (PDB entry 2NX3, chain J). (B) *Pfu*DAH7PS (PDB entry 1ZCO, E4P modeled by Schofield et al.[6]). Carbon atoms are colored green. In both structures, the $\beta7\alpha7$ loop is colored cyan, the $\beta8\alpha8$ loop is colored magenta, and the $\beta2\alpha2$ loop is colored yellow.

create the A5P binding site, and support intersubunit contacts in the tetrameric protein.

The $\beta8\alpha8$ loop bends toward the active site and provides a conserved and critical metal ligand Asp residue that also interacts with the C3-OH group of A5P. It has been suggested that as the reaction between PEP and A5P proceeds, this Asp may act as a proton source for the A5P carbonyl.[19] However, other studies have suggested the possibility that this role of proton donor may be fulfilled instead by a nearby conserved Lys residue, present on the $\beta2\alpha2$ loop, in a mechanism similar to what has been proposed for DAH7P synthases, as we have recently reported.[20]

A conserved KANR(S/T) motif is present on the $\beta2\alpha2$ loop and is directly responsible for binding A5P.[9] The Lys of this motif is positioned near the carbonyl oxygen of A5P and, rather than the Asp on the $\beta8\alpha8$ loop, may provide a proton to the nascent hydroxyl group. The Asn residue interacts with the C2- and C4-OH groups of A5P and has been shown to be an important determinant for the C2-OH configuration requirements of KDO8P synthases.[20,21] The Arg and Ser/Thr bind the phosphate moiety of A5P. The residues equivalent to this motif in DAH7P synthases are contained in an equally conserved but shorter KPR(S/T) motif, where the roles of Lys, Arg, and Ser/Thr are the same. Swapping the KANR(S/T) motif with the KPR(S/T) motif is by itself not sufficient to allow KDO8P synthase to use E4P as a substrate.[20]

A notable difference between KDO8P synthases and DAH7P synthases is highlighted by sequence and structural alignments that indicate a long or extended $\beta7\alpha7$ loop is always present in KDO8P synthases yet is not found in DAH7P synthases (Figure S1 of the Supporting Information).[22] This substantial sequence difference between the two enzymes represents a clear conserved difference in the construction of the binding sites for A5P and E4P. In KDO8P synthases, this $\beta7\alpha7$ loop is defined in crystal structures only when A5P and PEP are bound. Additionally, under these conditions, only two of the four active sites in the tetrameric assembly are observed to bind A5P simultaneously, suggesting that in KDO8P synthase catalysis may take place at alternating active sites.[9]

Initially, it was proposed that the $\beta7\alpha7$ loop played a role in shielding the active site from bulk solvent, to prevent the undesirable reaction of PEP with water.[23] Recently, however, it was found that mutation of a conserved Arg on loop $\beta4\alpha4$, which interacts with loops $\beta2\alpha2$ and $\beta7\alpha7$ across a subunit interface and contributes to the binding of the A5P phosphate moiety, impaired closure of the $\beta7\alpha7$ loop, without leading to the unproductive reaction of PEP with water.[22] The role of this conserved difference in loop $\beta7\alpha7$ between KDO8P synthase and DAH7P synthase remains unclear.

In this study, we have directly examined the role of the $\beta7\alpha7$ loop in KDO8P synthase activity, via its removal to match the active-site architecture of DAH7P synthase and via the mutation of the two absolutely conserved residues of this loop, a Gln and a Ser. Our results indicate that the extent of catalysis by both metal-dependent and metal-independent enzymes is significantly diminished by one mutation, the other, or both mutations and that catalysis is almost completely abrogated in the absence of this loop. The multiple interactions provided by this extended loop are required to support efficient catalysis by KDO8P synthase.

EXPERIMENTAL PROCEDURES

Bacterial Strains, Plasmids, Media, and Growth Conditions. The proteins in this study were expressed and purified using methods previously described.[7,20,24] *Escherichia coli* BL21(DE3) Star cells containing plasmids encoding the genes for the proteins were grown until the OD_{600} reached 0.4−0.8 at 37 °C. Gene expression was under the control of a T7 promoter, and expression was induced with the addition of IPTG to a final concentration of 1 mM. Cells were harvested 4 h postinduction or were cooled to 23 °C immediately after induction and harvested the following morning.

Site-Directed Mutagenesis. Mutants of *Nme*KDO8PS and *Afe*KDO8PS were generated by site-directed mutagenesis

dx.doi.org/10.1021/bi201231e | *Biochemistry* 2011, 50, 9318−9327

using a Quikchange II Lightning Site-Directed Mutagenesis Kit (Stratagene) in the case of *Nme*Q202A, *Nme*S211A, *Nme*Q202A/S211A, *Afe*Q198A, *Afe*S207A, and *Afe*Q198A/S207A. The primers listed in Table 1 were used to generate

Table 1. Mutant Oligonucleotide Primer Sequences

oligonucleotide	sequence (5′−3′)
*Afe*Q198A	GATGCGACCCATTCCGTAGCGCTCCCCGGTG
*Afe*Q198A	CACCGGGGAGCGCTACGGAATGGGTCGCATC
*Afe*S207A	AGGGTGACCGGGCCGGAGGCCAG
*Afe*S207A	CTGGCCTCCGGCCCGGTCACCCT
*Nme*Q202A	GTTACCCATTCCCTGGCAACCCGCGATGCCGG
*Nme*Q202A	CCGGCATCGCGGGTTGCCAGGGAATGGGTAAC
*Nme*S211A	GCCGGTTCTGCCGCAGCCGGCGGT
*Nme*S211A	ACCGCCGGCTGCGGCAGAACCGGC
*Afe*L7trun	CATTCCGTAGGCCAGCGCGAATTTATCC
*Afe*L7trun	GCGCTGGCCTACGGAATGGGTCGCATCA
*Nme*L7trun	CATTCCCTGGGTCGTCGCGCACAGGCTTTG
*Nme*L7trun	GCGACGACCCAGGGAATGGGTAACGTCG

these mutants using the pT7-7-*Nme*KDO8PS and pT7-7-*Afe*KDO8PS plasmids as templates, or in the case of the double mutants, pT7-7-*Nme*KDO8PS-S211A and pT7-7-*Afe*KDO8PS-Q198A.

$\beta 7\alpha 7$ loop stitch-out mutants (L7trun) were created by polymerase chain reaction (PCR) using complementary primers in the stitch-out region, which contained an 18-nucleotide 5′-complementary sequence that comprised a nine-nucleotide region immediately upstream of the 5′ end of the fragment to be deleted and a nine-nucleotide region immediately downstream of the 3′ end. Therefore, the linear PCR products contained an overlapping sequence of 18 nucleotides at the 5′ and 3′ ends, which allowed them to be circularized into viable plasmids after in vivo recombination in transfected *E. coli*. For the *Afe*L7trun and *Nme*L7trun mutants, this corresponded to deletion of amino acids Q198−G208 and Q202−G212, respectively. The *Nme*L7trun-KPRS and *Afe*L7trun-KPRS (KPRS is the combination of A58P with N59del and A56P with N57del, respectively) mutants were created using previously described methods,[20] with the respective L7trun mutant sequences as the templates.

Enzyme Purification and Assays. All proteins were purified by a three-step procedure of anion exchange, followed by hydrophobic interaction and then size-exclusion chromatography, as previously described.[7,20,24] The enzyme assay used for KDO8PS has been previously described.[7,24] Briefly, the consumption of PEP is monitored at 232 nm ($\varepsilon = 2.8 \times 10^3$ M^{-1} cm^{-1} at 37 °C), and the initial rates of reaction were determined by a least-squares fit. A unit of enzyme activity was defined as the loss of 1 μmol of PEP/min at 37 °C.

Michaelis−Menten Kinetics. The assays for determining the kinetic parameters kept the concentration of one substrate constant while varying that of the other and vice versa. The amount of KDO8PS used in each assay ranged from 0.02 to 0.08 mg depending on the experiment. To determine K_m^{PEP}, the A5P concentration was kept at 150 μM, and the concentration of PEP was varied from 2.8 to 98 μM for all Q to A and S to A mutants, except for *Afe*Q198A/S207A and *Afe*S207A for which the A5P concentration was 854 μM and the PEP concentration varied from 8.5 to 204 μM and from 4.3 to 85 μM, respectively. For *Nme*Q202A/S211A, the A5P concentration was 1768 μM and the PEP concentration varied between 2.6 and 63 μM. To determine K_m^{A5P} for these mutants, the PEP concentration was kept at 100 μM and the A5P concentration was varied between 6.4 and 205 μM, 102 and 411 μM, and 26 and 411 μM for *Nme*S211A, *Nme*Q202A, and *Afe*Q198A, respectively. For *Afe*Q198A/S207A, *Afe*S207A, and *Nme*Q202A/S211A, the PEP concentration was 150 μM and the A5P concentration was varied between 24 and 488 μM for both *Afe*Q198A/S207A and *Afe*S207A and between 110 and 384 μM for *Nme*Q202A/S211A. For the K_m^{A5P} determinations for the L7trun enzymes, the PEP concentration was kept constant at 150 μM and the A5P concentration was varied between 500 μM and 3 mM for *Nme*L7trun and between 200 μM and 3 mM for *Afe*L7trun. The amount of KDO8P produced by the L7trun proteins was measured using the periodate−thiobarbituric acid assay[25] to rule out uncoupled hydrolysis of PEP. The two L7trun mutant proteins produced the same amount of KDO8P as the wild-type enzymes. Assays for determining the activity of the L7trun-KPRS enzymes used 150 μM PEP and 1 mM A5P.

Isothermal Titration Calorimetry. Binding of *Afe*KDO8PS mutants to PEP was assessed by isothermal titration calorimetry (ITC) using a VP-ITC unit operating at 298 K (Microcal, GE Healthcare). Before use, proteins were buffer-exchanged against binding buffer and all solutions degassed in a vacuum. All concentrations were measured by UV absorption at 280 nm ($\varepsilon_{AfeKDO8PS}$ = 17335 M^{-1} cm^{-1}, and $\varepsilon_{NmeKDO8PS}$ = 6335 M^{-1} cm^{-1}) immediately before titrations were started. For *Afe*KDO8PS, the binding buffer consisted of 50 mM BTP (pH 7.0) and 0.5 mM $MnSO_4$ and titrations comprised 29 injections of ligand, one 2 μL injection followed by 28 10 μL injections. The protein concentration in the cell was 0.65 μM, and the PEP concentration in the syringe was 0.065 μM. For *Nme*KDO8PS, the binding buffer consisted of 50 mM BTP (pH 7.0) and titrations comprised 27 injections of ligand, one 2 μL injection followed by 26 10 μL injections. The protein concentration in the cell was 110 μM, and the PEP concentration in the syringe was 2 mM. The initial datum was routinely deleted to allow for diffusion of ligand and/or receptor across the needle tip during the equilibration period. Heat of dilution experiments were conducted independently and the data subtracted from the integrated data before curve fitting in Origin 7.0 with the standard one-site model supplied by Microcal.

Crystallization. Crystals of *Nme*Q202A, *Nme*S211A, *Nme*L7trun, and *Nme*L7trun-KPRS were grown by hanging drop vapor diffusion. Protein was mixed 1:1 (v/v) with reservoir solution containing 100 mM sodium acetate (pH 4.6) and 0.6−2.8 M NaCl. The drop volume was 2 μL and the reservoir solution volume 500 μL. The crystallization trays were left at 20 °C until immediately before data collection, when crystals were transferred briefly into a cryoprotectant solution composed of 20% glycerol in the respective reservoir solution. Crystals typically began to form after 4 h and were fully formed after 24 h. Although crystallization was attempted in the presence of substrates, no evidence of ligand binding to the crystals was observed. It is likely that the low pH of the crystallization condition hinders ligand binding.[7]

Structure Determination and Refinement. For *Nme*Q202A and *Nme*S211A, a Rigaku MicroMax007 microfocus copper rotating anode generator with AXCo PX70 focusing capillary optic (λ = 1.5418 Å) coupled with an R-AxisIV^{++} image plate detector was used to collect data sets at 120 K (Oxford Cryosystems Series 700). Data collection and

Table 2. Crystal Parameters and Data Collection and Refinement Statistics

	*Nme*Q202A	*Nme*S211A	*Nme*L7trun	*Nme*L7trun-KPRS
		Data Collection		
crystal system, space group	orthorhombic, $P2_12_12_1$	orthorhombic, $P2_12_12_1$	orthorhombic, $P2_12_12_1$	orthorhombic, $P2_12_12_1$
unit cell parameters *a*, *b*, *c* (Å)	81.84, 85.74, 163.30	82.19, 85.83, 163.30	81.78, 85.76, 163.22	81.69, 104.05, 149.62
resolution range (Å)	30.56−2.05 (2.12−2.05)	36.87−1.90 (1.96−1.90)	37.99−1.91 (2.01−1.91)	38.01−2.20 (2.32−2.20)
no. of measurements	305089	294670	522701	480225
no. of unique reflections	72315	86379	88598	65469
redundancy	4.22 (4.17)	3.41 (3.25)	5.9 (4.9)	7.3 (7.4)
completeness (%)	99.3 (99.9)	93.7 (94.3)	99.5 (99.1)	100 (100)
$I/\sigma(I)$	4.8 (1.6)	5.2 (1.6)	8.2 (1.9)	7.4 (1.8)
R_{merge} (%)	0.067 (0.383)	0.062 (0.376)	0.062 (0.313)	0.087 (0.347)
Wilson *B* value (Å^2)	34.8	32.8	22.2	24.0
		Refinement		
resolution (Å)	30.60−2.05	36.87−1.90	36.56−1.91	35.99−2.20
R_{cryst}	0.2049	0.2203	0.2092	0.2083
R_{free}	0.2474	0.2584	0.2453	0.2448
chain length	280	280	269	268
no. of observed residues	250 + 249 + 253 + 254 residues; 7739 atom sites	250 + 251 + 252 + 251 residues; 7733 atom sites	249 + 254 + 260 + 259 residues; 7906 atom sites	260 + 268 + 260 + 258 residues; 8138 atom sites
no. of water molecules	534	586	699	574
no. of other molecules	1 Cl^-, 1 Na^+	1 Cl^-, 1 glycerol, 1 Na^+	7 (1 × 0.67) Cl^-, 1 Na^+	12 Cl^-
mean *B* (Å^2)				
protein	39.12	41.72	31.07	24.86
water	39.52	38.43	33.13	24.08
other	39.51	44.08	33.52	28.50
rmsd from target values				
bond lengths (Å)	0.010	0.012	0.011	0.013
bond angles (deg)	1.102	1.215	1.158	1.267
dihedral angles (deg)	5.376	5.274	5.107	5.427
Ramachandran plot				
most favored (%)	93.3	93.9	94.2	93.3
allowed (%)	5.5	5.1	4.9	5.8
generously allowed (%)	0.9	0.7	0.6	0.7
disallowed (%)	0.2	0.3	0.3	0.2
PDB entry	3STE	3STF	3STC	3STG

processing were performed with CrystalClear.[26] Data sets for *Nme*L7trun and *Nme*L7trun-KPRS were collected at the Australian Synchrotron using the Macromolecular Crystallography (MX1) beamline and were processed using iMosFlm 1.0.4 and SCALA (CCP4 suite).[27,28] The results are summarized in Table 2, along with key structure refinement details. Data were collected for crystals of *Nme*Q202A grown in a 0.8 M NaCl condition, *Nme*S211A in 1.0 M NaCl, *Nme*L7trun in 1.6 M NaCl, and *Nme*L7trun-KPRS in 2.8 M NaCl. All four mutant proteins crystallize, like the wild type, in orthorhombic space group $P2_12_12_1$ with the following unit cell dimensions: $a \approx 82$ Å, $b \approx 85$ Å, and $c \approx 163$ Å. The exception is *Nme*L7trun-KPRS, which had the following unit cell dimensions: $a = 82$ Å, $b = 104$ Å, and $c = 150$ Å. Crystals diffracted to 2.05, 1.90, 1.90, and 2.20 Å, respectively. The wild-type *Nme*KDO8PS structure (PDB entry 2QKF) was used to determine the structure of *Nme*Q202A and *Nme*S211A, and a modified wild-type structure with the excised $\beta7\alpha7$ loop residues removed from the PDB file was used for the solution of *Nme*L7trun, both carrying through the same set of reflections for calculation of R_{free}. The *Nme*L7trun model was used with Phaser[29] to determine the structure of *Nme*L7trun-KPRS by molecular replacement, with the same R_{free} reflection set. Refinements were conducted with Refmac5,[30] and electron density maps were analyzed with COOT.[31] The validation tools of COOT and Molprobity were used to check for, and correct, conformational infelicities. All diagrams were drawn with PyMol.

Molecular Modeling of the Interactions of the $\beta7\alpha7$ Loop with the Linear Tetrahedral Intermediate. A complete model of *Nme*KDO8PS, including the regions of the original structure that were poorly defined in the crystal structure of the wild-type protein,[7] was built by homology modeling using Prime.[32] The model was constructed using the

comparative method, using the two template structures, PDB entries 2QKF (*Nme*KDO8PS) and 1FWW [*Aquifex aeolicus* KDO8PS (*Aae*KDO8PS)]. PDB entry 1FWW was used as a template for the missing loops of the *Nme*KDO8PS structure and loop $\beta2\alpha2$; these include residues 53−72, 200−218, and 237−257 (numbering of PDB entry 2QKF). The substrates PEP and A5P that were bound in 1FWW were retained in the homology model. All other residues of *Nme*KDO8PS were built using PDB entry 2QKF as the template. Each monomer was built separately using the corresponding chain in 2QKF and chain A of 1FWW. The four monomers were then assembled to form the tetrameric complex. The tetramer was then minimized with Prime, to optimize bond lengths and bond angles and to remove steric clashes.

The structures of both possible diastereoisomers of the tetrahedral intermediate were built in Maestro[33] of Schrödinger Suite 2010 and then minimized with MacroModel.[34] A conformational search for each isomer was then conducted using the MCMM Serial Torsional Sampling method. The lowest-energy conformer of each isomer was used in the docking calculations as the starting conformation. The modeling of the tetrahedral intermediate diastereoisomers into the active site of *Nme*KDO8PS was conducted with the Schrödinger Suite 2010 Induced Fit Docking protocol.[35−37] The active site in chain A of the homology model (with ligands removed) was used as the receptor. The center of the receptor grid was defined as the centroid of residues 23, 52, 54, 57, 59−62, 65, 92, 94, 110−114, 135, 165, 196, 199, 202, 204, 205, 209−211, 234, 236, 246, 247, and 250 in chain A and residue 117 in chain C. For the initial docking, the van der Waals radii of the atoms on the tetrahedral intermediate were scaled to 0.8. The 20 best solutions of initial docking were kept. All residues on the enzyme within a 5 Å distance of the respective docked pose were refined. The ligands were redocked to the top 20 newly generated protein structures if the energy was within 30 kcal/mol of that of the best pose. A schematic of the tetrahedral intermediate is shown as part of Figure 6A.

RESULTS

Expression, Purification, and Stability. Relative to the short loop linking $\beta7$ and $\alpha7$ in DAH7P synthase, the $\beta7\alpha7$ loop of both metal-dependent and metal-independent KDO8P synthases is extended by 11 residues (Figure 3). Two of these residues, Gln and Ser, at the beginning and near the end of the loop, respectively, are absolutely conserved in KDO8P synthases. The structure of the *A. aeolicus* KDO8P synthase enzyme in complex with PEP and A5P indicates contacts are made between the Gln and C3-OH group of A5P and between the Ser and the A5P phosphate functionality.

To probe the role of the conserved Gln and Ser residues in the extended $\beta7\alpha7$ loop of KDO8P synthase, these residues were mutated to Ala in both a metal-dependent KDO8P synthase from *Acidithiobacillus ferrooxidans* (*Afe*KDO8PS) and metal-independent KDO8P synthase from *Neisseria meningitidis* (*Nme*KDO8PS) (creating *Nme*Q202A, *Nme*S212A, *Afe*Q198A, and *Afe*S207A). Double-mutant proteins containing both the Gln-to-Ala and Ser-to-Ala substitutions (*Nme*Q202A/S212A and *Afe*Q198A/S207A) were also created. Additionally, the 11 extra residues of this extended loop were excised from both proteins to make them resemble this loop's length in DAH7P synthase, creating *Nme*L7trun and *Afe*L7trun. These truncated enzymes were further modified in the $\beta2\alpha2$ loop region, via alteration of the absolutely conserved LysAlaAsnArgSer

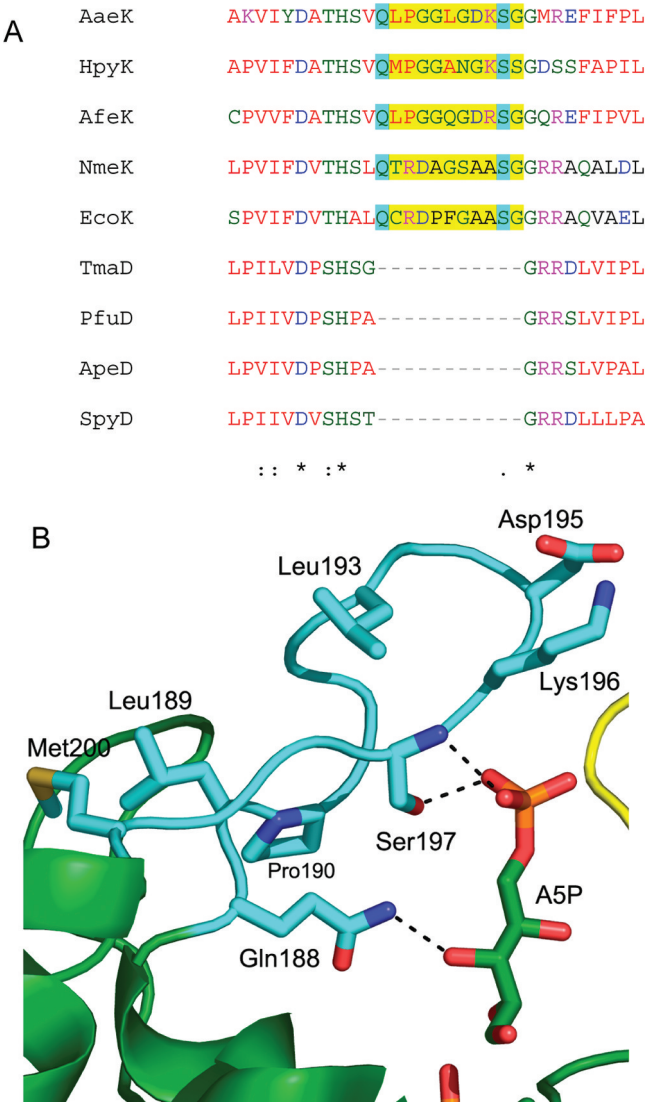

Figure 3. (A) Partial sequence alignment of KDO8P synthase and type Iβ DAH7P synthase sequences showing the additional amino acids that extend the $\beta7\alpha7$ loop in KDO8P synthases. The regions corresponding to those excised in *Nme*KDO8PS and *Afe*KDO8PS are highlighted in yellow, inclusive of the two conserved residues of the $\beta7\alpha7$ loop, which are highlighted in cyan. KDO8P synthases are denoted as XyzK and DAH7P synthases as AbcD. Full names for the organisms are provided in the figure legend of Figure S1 of the Supporting Information. (B) Expansion of the $\beta7\alpha7$ loop of *Aae*KDO8PS. In this study, the absolutely conserved Gln and Ser of loop 7 (equivalent to Gln188 and Ser197 of *Aae*KDO8PS, respectively) were mutated to Ala in *Nme*KDO8PS and *Afe*KDO8PS, creating *Nme*Q202A, *Nme*S211A, *Nme*Q202A/S211A, *Afe*Q198A, *Afe*S207A, and *Afe*Q198A/S211A.

(KANRS) motif of KDO8PS to the equivalent LysProArgSer (KPRS) motif found for DAH7PS proteins.

The mutants were constructed and purified using the same methods that were used for the respective wild-type proteins. Sequencing of the mutated plasmids and the mass spectra of the proteins confirmed the successful alterations to the sequences. Measurement of the circular dichroism spectra of the mutated *Afe*KDO8PS proteins indicated that the introduced mutations had caused no gross structural perturbations (Figure S2 of the Supporting Information). Denaturation temperatures measured by differential scanning fluorimetry for the $\beta7\alpha7$

Table 3. Kinetic Parameters of Wild-Type and $\beta7\alpha7$ Loop Mutant *Nme*KDO8PS and *Afe*KDO8PS[a]

protein	K_m^{PEP} (μM)	K_m^{A5P} (μM)	k_{cat} (s^{-1})	k_{cat}/K_m^{A5P} (s^{-1}/mM)
wild-type *Nme*	2.5 ± 0.2	12.0 ± 0.5	8.0 ± 0.1	670 ± 40
*Nme*Q202A	7 ± 1	160 ± 20	3.6 ± 0.2	23 ± 4
*Nme*S211A	3.6 ± 0.9	74 ± 10	6.2 ± 0.3	80 ± 20
*Nme*Q202A/S211A	9 ± 1	300 ± 18	3.8 ± 0.2	13 ± 1
*Nme*L7trun		3900 ± 100	0.46 ± 0.01	0.118 ± 0.007
*Nme*L7trun-KPRS	–	–	–	–
wild-type *Afe*	12 ± 1	22 ± 2	4.8 ± 0.1	220 ± 20
*Afe*Q198A	11 ± 1	151 ± 13	3.1 ± 0.2	21 ± 3
*Afe*S207A	6.8 ± 0.3	153 ± 17	2.53 ± 0.03	17 ± 2
*Afe*Q198A/S207A	59 ± 3	173 ± 23	1.38 ± 0.03	8 ± 1
*Afe*L7trun		480 ± 20	0.0728 ± 0.0008	0.151 ± 0.007
*Afe*L7trun-KPRS	–	–	–	–

[a]Enzymes with no measurable activity (k_{cat} < 0.001 s^{-1}) are denoted with dashes.

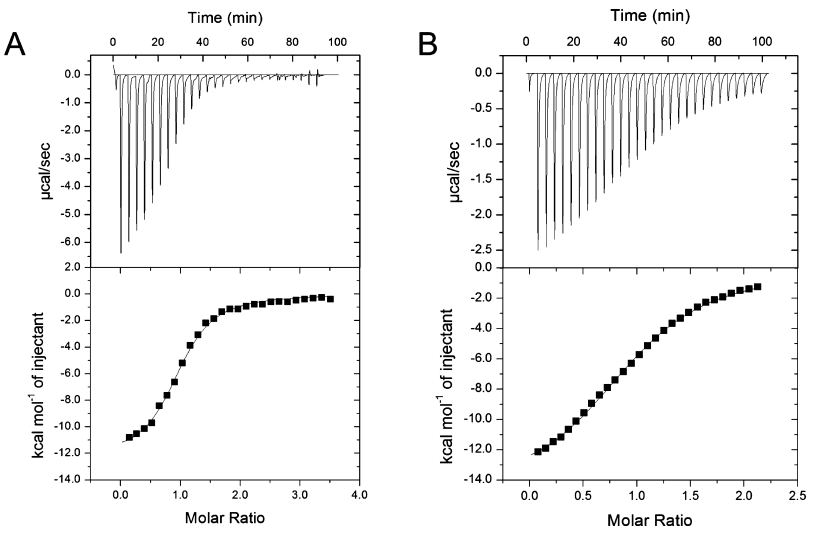

Figure 4. Quantification of binding interactions of loop $\beta7\alpha7$-truncated mutants of *Nme*KDO8PS and *Afe*KDO8PS with PEP by ITC. Data were fitted with a simple one-site binding model. (A) For *Nme*L7trun, K_D = 11.8 ± 0.8 μM. (B) For *Afe*L7trun, K_D = 13.6 ± 0.4 μM.

loop-truncated proteins of both *Nme*- and *Afe*KDO8PS (Table S2 of the Supporting Information) were also measured. The denaturation temperatures for the *Nme*KDO8PS $\beta7\alpha7$ loop-truncated protein were similar to those of the wild type, and the presence of Cd^{2+}, which had been previously shown to result in a substantial reduction in the denaturation temperature of the wild-type enzyme,[24] remained strongly destabilizing. The *Afe*KDO8PS $\beta7\alpha7$ loop-truncated protein was less stable under all conditions, showing a denaturation temperature lower than that of wild-type *Afe*KDO8PS.

Kinetic Characterization. The single- and double-mutant proteins and full loop truncations (*Nme*L7trun and *Afe*L7trun) all retained some ability to catalyze the KDO8P synthase reaction (Table 3). However, the proteins in which the $\beta7\alpha7$ loop had been removed catalyzed the KDO8P synthase reaction very poorly. For all active mutant enzymes, K_m^{PEP} was similar to that measured for the respective wild-type enzyme. In contrast, the K_m^{A5P} values were higher than those recorded for the wild type, consistent with the mutated regions of the proteins making weaker interactions with this substrate. For *Afe*KDO8PS, both single and double substitutions with Ala of the conserved Gln and Ser of the $\beta7\alpha7$ loop resulted in similar ~7- and 8-fold increases in K_m^{A5P}, respectively, relative to that of the wild-type enzyme. On the other hand, for *Nme*KDO8PS, there are 6-, 12-, and 24-fold increases in K_m^{A5P} for mutants S212A, Q202A, and Q202A/S212A, respectively, relative to that of the wild-type enzyme, suggesting that in this enzyme the binding interactions provided by the Ser to A5P are less important that those provided by the Gln.

In marked contrast to the modest loss of catalytic activity of the single and double mutants, the truncated proteins (*Nme*L7trun and *Afe*L7trun), without the extended $\beta7\alpha7$ loop, exhibited very low activity. K_m^{A5P} values were much larger, and the k_{cat} values for these enzymes were significantly lower. For the metal-independent *Nme*KDO8PS enzyme, the change in specific activity was more substantial: the k_{cat}/K_m^{A5P} was found to be more than 5700 times lower for the truncated protein than for the wild-type enzyme (compared to 1400 times lower for the metal-dependent *Afe*KDO8PS). There was no measurable activity for the proteins that combined the $\beta7\alpha7$ loop truncation with the mutation of the conserved KANRS motif, to the equivalent KPRS motif conserved in DAH7P synthase (L7trun-KPRS). Nor was there activity for these L7trun-KPRS mutated enzymes with ribose 5-phosphate, 2-deoxyribose 5-phosphate, or E4P used in place of A5P.

The binding interactions of PEP with the $\beta7\alpha7$ loop-truncated proteins were measured by ITC. Compared to measurements on the wild-type protein (for *Afe*KDO8PS, K_D = 5.0 ± 0.1 μM; for *Nme*KDO8PS, K_D = 4.8 ± 0.2 μM), the PEP binding to the truncated proteins is significantly but not greatly

dx.doi.org/10.1021/bi201231e | *Biochemistry* 2011, 50, 9318–9327

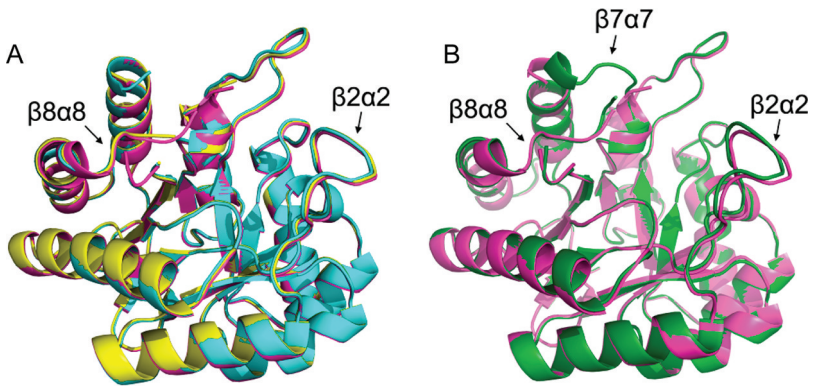

Figure 5. (A) Overlay of the structures of *Nme*Q202A (yellow), *Nme*S211A (cyan), and wild-type *Nme*KDO8PS (magenta). (B) Overlay of the structures of *Nme*L7trun (green) and wild-type *Nme*KDO8PS (magenta). The $\beta 8\alpha 8$ loop is partially ordered in all structures, and the $\beta 7\alpha 7$ loop is ordered only in *Nme*L7trun. Subunit C has been used in each superposition.

impaired (for *Nme*L7trun, $K_D = 11.8 \pm 0.8$ μM; for *Afe*L7trun, $K_D = 13.6 \pm 0.4$ μM) (Figure 3), indicating that the primary effect of the deletion of the $\beta 7\alpha 7$ loop was to impair the interaction of A5P with the protein.

Crystallography. The *Nme*KDO8PS mutant proteins crystallized in the same way as the wild-type enzyme with one complete tetramer per asymmetric unit. In the structure of wild-type *Nme*KDO8PS (and those of its mutants), the residues of loop $\beta 7\alpha 7$ are disordered from Gln202 (or Thr203) to at least Gly213 in all four subunits. In the structure of *Nme*Q202A (rmsd of Cα atoms on the superimposed wild-type structure of 0.161 Å), there are no observed differences compared to the wild-type structure. The only exception is for the Q202A mutation, which, as in the wild-type structure, is the last ordered residue of the $\beta 7\alpha 7$ loop. Likewise, the structure of *Nme*S211A is very similar to the wild-type structure (rmsd = 0.233 Å). However, for this mutant, loop $\beta 2\alpha 2$ of chain D has shifted away from the active site between residues Asn59 and Val69, and in chain B, the side chain of Glu236 now reaches into the space usually occupied by His199 and that of His199 has moved to a space sometimes occupied by alternative conformations of Arg165. The mutation of Ser211 to Ala is in the region of loop $\beta 7\alpha 7$ that is disordered in the wild type and all nontruncated mutant structures.

The structure of *Nme*L7trun is also very similar to the wild-type structure, but the rmsd of 0.401 Å, while modest, is significantly greater than that for superposition of single and double mutants on the wild-type enzyme, indicating that there are small changes induced by the truncation. The most notable of these changes is a small twist at the end of helix 7, which is likely constrained relative to the wild-type protein because of the shortened $\beta 7\alpha 7$ loop (Figure 5). However, for the first time, except for KDO8P synthase from hyperthermophilic organisms, the truncated $\beta 7\alpha 7$ loop is ordered in all four subunits. In chain B, as was observed for *Nme*S211A, the side chains of His199, Glu228, and Arg165 have likewise rearranged, suggesting that in the absence of substrates there is some flexibility in the positioning of these side chains.

The *Nme*L7trun-KPRS mutant protein crystallized in the same space group as all previous *Nme*KDO8PS structures but with different unit cell dimensions. The crystal structure is very similar to that of *Nme*L7trun (rmsd = 0.401 Å). In all *Nme*KDO8PS structures, both the (nontruncated) $\beta 7\alpha 7$ and $\beta 8\alpha 8$ loops are normally disordered. For the first time in a structure of *Nme*KDO8PS, the main chain of the $\beta 8\alpha 8$ loop has become ordered (in chain B). This is likely a result of tighter crystal packing in the new unit cell; the $\beta 8\alpha 8$ loop of chain B contacts helix $\alpha 1$ and loop $\alpha 2\beta 3$ from an adjacent tetramer. Asp235 on the $\beta 8\alpha 8$ loop, which corresponds to the metal ligand in metal-dependent KDO8P synthases, is pointing away from the active site and is hydrogen bonding to His228. Although the orientation observed here is an unproductive conformation and is likely present only because of the absence of substrates and because of crystal packing effects, it almost certainly represents an orientation sampled in solution in the absence of substrates. The tighter packing between tetramers has also ordered the usually conformationally variable $\beta 2\alpha 2$ loop into a common conformation in all four monomers, with the conserved Arg59 (Arg60 in wild-type enzyme mutants retaining the KANRS motif) always pointing toward the active site. In contrast, in the structure of *Nme*L7trun, in three of four chains, Arg60 is in an unproductive orientation, hydrogen bonding to Asp120 of the adjacent monomer, which normally is observed to hydrogen bond to Arg69 at the end of the $\beta 2\alpha 2$ loop.

Modeling of the Reaction Intermediate. To examine the possible interactions between the substrates and the residues of the $\beta 7\alpha 7$ loop, the proposed tetrahedral intermediate for the KDO8P synthase reaction was modeled into *Nme*KDO8PS using induced fit docking. The study produced a total of 28 poses for the two isomers of the tetrahedral intermediate in the active site of *Nme*KDO8PS; two poses retained the expected PEP binding interactions. Both the poses with the correct PEP orientation are from the *S*-isomer of the tetrahedral intermediate. In the best pose, the PEP part of the molecule interacts with residues Arg165, Lys135, Gln110, Lys52, and Lys57 and the backbone of Ala113 (Figure 6). The A5P phosphate group interacts with Arg60 and Ser61 (from the $\beta 2\alpha 2$ loop), Asp205, Ser211, and the backbone of Ala209 (from the $\beta 7\alpha 7$ loop), and Arg117 (extending from the adjacent subunit). The hydroxyl groups derived from A5P are held in place by hydrogen bonding to Asn59, Asp247, and Gln202. The A5P aldehyde group, now converted to a hydroxyl group in the tetrahedral intermediate, interacts with Lys57, Asn23, and His199. The OH group that corresponds to the incoming water molecule forms an H-bond with the side chain of Gln110. These interactions bear close correspondence to those modeled from crystallographic observations for the intermediate in *Aae*KDO8PS (PDB entry 2NX3 chain D).[13]

dx.doi.org/10.1021/bi201231e | *Biochemistry* 2011, 50, 9318–9327

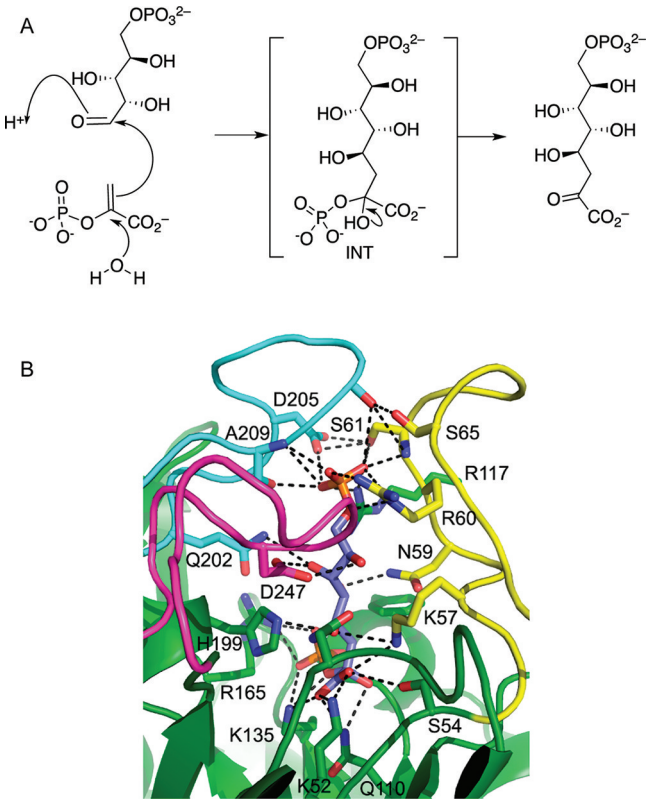

Figure 6. (A) Existence of this tetrahedral intermediate that has been demonstrated by mass spectral studies.[38] (B) Proposed tetrahedral intermediate (purple) for the KDO8P synthase reaction modeled into the active site of *Nme*KDO8PS. Carbon atoms are colored green. The carbon atoms of the $\beta7\alpha7$ loop are colored cyan, those of the $\beta8\alpha8$ loop magenta, and those of the $\beta2\alpha2$ loop yellow.

It is clear from these studies that the interactions between residues arising from the extended $\beta7\alpha7$ loop and A5P are extensive and involve more residues of this loop than the absolutely conserved Gln202 and Ser211. In addition, hydrogen bonds between the $\beta7\alpha7$ and $\beta2\alpha2$ loops are observed. Specifically, Ser61 hydrogen bonds to Asp209, and Ser65 interacts with the main chain carbonyl oxygen of Ala209.

DISCUSSION

Variants of *Nme*KDO8PS and *Afe*KDO8PS created by excising the extended $\beta7\alpha7$ loop were found to have severely attenuated catalytic activity. This compromise of activity was far more significant than that which resulted from the removal of the side chains of the two absolutely conserved residues, Gln and Ser, of this loop. This loop has little effect on PEP binding, but in line with the experimental studies that indicate the importance of the extended $\beta7\alpha7$ loop for A5P binding, modeling studies predict that the $\beta7\alpha7$ loop interacts extensively with A5P and also helps to buttress the position of the $\beta2\alpha2$ loop. This latter loop supports multiple key interactions with A5P and provides a catalytically essential Lys residue.[20]

The $\beta7\alpha7$ loop is conserved for all KDO8P synthases regardless of their metal dependency; however, the relative importance of the $\beta7\alpha7$ loop for efficient catalysis and binding of A5P does appear to depend on the metal dependency of the enzyme. The metal-dependent *Afe*KDO8PS was noticeably less compromised by the truncation of the $\beta7\alpha7$ loop than the metal-independent *Nme*KDO8PS, or for that matter by mutation of the conserved residues. The metal ion appears then to play a role in supporting the correct placement of A5P for reaction, and it is conceivable the metal-dependent enzymes may be less reliant on the extended $\beta7\alpha7$ loop for accurate A5P binding. Together, these observations appear to reflect an evolution of the metal-independent forms from a metal-dependent ancestor, which in turn evolved from the metal-dependent type Iβ DAH7P synthases.

What remains striking and unexplained is the fact that no extant DAH7P synthase has an extended $\beta7\alpha7$ loop and no extant KDO8P synthase has a truncated $\beta7\alpha7$ loop. The absence of this loop has little effect on PEP binding, but its presence is associated with a change in substrate specificity, from the four-carbon E4P for DAH7P synthase to the five-carbon A5P for KDO8P synthase. The longer and more flexible A5P substrate may require additional contacts to bind competently to the enzyme and to help ensure correct substrate selection. DAH7P synthase, on the other hand, uses a less flexible $\beta2\alpha2$ loop (compared to its counterpart in KDO8P synthase) to provide the necessary contacts to ensure effective E4P binding. The presence of the extended $\beta7\alpha7$ loop in KDO8P synthase might indicate that the determining factor in the evolution of KDO8P synthase was the acquisition of the 11-residue $\beta7\alpha7$ loop insertion. Curiously, the KDO8P synthase from *Helicobacter pylori* has a second 12-residue extension in the $\beta6\alpha6$ loop, indicating, perhaps, that loop extension is genetically facile.

In crystal structures of both metal-dependent and metal-independent KDO8P synthase, the $\beta7\alpha7$ loop is often disordered and becomes visible only in structures with both PEP and A5P bound, as in the KDO8P synthase from the thermophile *A. aeolicus*.[9] The apparent mobility of the loop maintains easy access to the active site for the substrates, as well as exit for the products, and when ordered and closed helps arrange and select the substrate. The extended loop is an additional tool for helping to orient the substrate properly, and the interactions it provides also act in concert with other active-site contacts, particularly the essential ones provided by the $\beta2\alpha2$ loop. The entropic cost of ordering a mobile $\beta7\alpha7$ loop as part of the catalytic cycle probably represents a compromise between facile active-site access and the need for added strategies for binding A5P, as is apparent in the Michaelis constants for metal-independent *Nme*KDO8PS compared to those of metal-dependent *Afe*KDO8PS, to ensure efficient catalysis and accurate substrate selection.

The distinctive ordering of the otherwise disordered $\beta8\alpha8$ loop observed in one subunit in the structure of L7trun-KPRS *Nme*KDO8PS provides, perhaps, a clue into controlling the entropic penalty of the ordering of long apparently flexible loops on substrate binding. The $\beta8\alpha8$ loop of this subunit traces approximately the path observed in substrate-bound *Aae*KDO8PS,[9] but changes in side chain conformations of absolutely conserved residues Asp235 and His228 on loop $\beta8\alpha8$ and also of Glu26 (*Nme*KDO8PS numbering) lead to alternative contacts with one another, compared to those contacts observed in substrate-bound *Aae*KDO8PS. Although the orientation observed here for Asp235 is an unproductive conformation and is likely present only because of the absence of substrates and is locked-in because of crystal packing effects, it almost certainly represents an orientation sampled in solution in the absence of substrates. The different uses of absolutely conserved residues by absolutely conserved residues on loop $\beta8\alpha8$ of *Nme*- and *Aae*KDO8PS provide a plausible resolution

of the paradox of the huge conformational entropy penalty when a flexible loop potentially sampling a multitude of conformations becomes locked into one productive conformation upon substrate binding: should this long $\beta 8\alpha 8$ loop sample only a small number of defined but very different conformations, as contrasted with a more continuous multitude of conformations, then the entropic penalty on binding substrates is greatly reduced. This reduced penalty need not increase if the conformations of one long potentially flexible loop are then correlated with another, such as loops $\beta 2\alpha 2$ and $\beta 7\alpha 7$ in nontruncated forms. It should be noted that more than a couple of conformations, even if very well ordered, are generally difficult to discern by X-ray diffraction techniques.

In summary, while the extended $\beta 7\alpha 7$ loop is not absolutely essential for catalysis by metal-dependent and metal-independent KDO8P synthase enzymes, its presence is necessary for efficient catalysis. This requirement for catalytic efficiency is not solely due to the interactions that involve the side chains of the absolutely conserved Ser and Gln residues of this loop but rather appears to demand the presence of the loop as a whole.

■ ASSOCIATED CONTENT

Ⓢ Supporting Information

An alignment of KDO8P synthase and DAH7P synthase sequences, the melt temperatures of wild-type and mutant *Nme*KDO8PS and *Afe*KDO8PS, circular dichroism spectra of wild-type and mutant *Afe*KDO8PS, and subunit molecular weights of wild-type and mutant *Nme*KDO8PS and *Afe*KDO8PS as determined by ToF-LCMS by ESI. This material is available free of charge via the Internet at http://pubs.acs.org.

Accession Codes

The atomic coordinates and structure amplitudes have been deposited with the Protein Data Bank as entries 3STE, 3STF, 3STC, and 3STG.

■ AUTHOR INFORMATION

Corresponding Author

*Department of Chemistry, University of Canterbury, Private Bag 4800, Christchurch, New Zealand. Telephone: (+64) 3 364 5682. Fax: (+64) 3 364 2110. E-mail: emily.parker@canterbury.ac.nz.

Funding

This research was funded, in part, by the New Zealand Marsden Fund (UOC0710). The College of Science of the University of Canterbury provided a Doctoral Scholarship for T.M.A., and the Rigaku MM007/RAxisIV^{++} X-ray generator and detector were funded by the Allan Wilson Centre for Molecular Ecology and Evolution. The Lottery Health Grants Board of New Zealand funded the capillary optic at Massey University.

■ ACKNOWLEDGMENTS

Part of this research was undertaken on the MX beamlines at the Australian Synchrotron, Victoria, Australia.

■ ABBREVIATIONS

A5P, D-arabinose 5-phosphate; *Aae*, *A. aeolicus*; *Afe*, *A. ferrooxidans*; BTP, 1,3-bis[tris(hydroxymethyl)methylamino]-propane; DAH7P, 3-deoxy-D-*arabino*-heptulosonate 7-phosphate; DAH7PS, 3-deoxy-D-*arabino*-heptulosonate 7-phosphate synthase; DSF, differential scanning fluorimetry; E4P, D-erythrose 4-phosphate; *Eco*, *E. coli*; IPTG, isopropyl β-D-thiogalactopyranoside; ITC, isothermal titration calorimetry; KDO, 3-deoxy-D-*manno*-octulosonate; KDO8P, 3-deoxy-D-*manno*-octulosonate 8-phosphate; KDO8PS, 3-deoxy-D-*manno*-octulosonate 8-phosphate synthase; LPS, lipopolysaccharide; *Nme*, *N. meningitidis*; PDB, Protein Data Bank; PEP, phosphoenolpyruvate; rmsd, root-mean-square deviation.

■ REFERENCES

(1) Levin, D. H., and Racker, E. (1959) Condensation of arabinose 5-phosphate and phosphoryl enol pyruvate by 2-keto-3-deoxy-8-phosphooctonic acid synthetase. *J. Biol. Chem. 234*, 2532−2539.

(2) Wyckoff, T. J., Raetz, C. R., and Jackman, J. E. (1998) Antibacterial and anti-inflammatory agents that target endotoxin. *Trends Microbiol. 6*, 154−159.

(3) Jensen, R. A., Xie, G., Calhoun, D. H., and Bonner, C. A. (2002) The correct phylogenetic relationship of KdsA (3-deoxy-D-*manno*-octulosonate 8-phosphate synthase) with one of two independently evolved classes of AroA (3-deoxy-D-*arabino*-heptulosonate 7-phosphate synthase). *J. Mol. Evol. 54*, 416−423.

(4) Subramaniam, P. S., Xie, G., Xia, T., and Jensen, R. A. (1998) Substrate ambiguity of 3-deoxy-D-*manno*-octulosonate 8-phosphate synthase from *Neisseria gonorrhoeae* in the context of its membership in a protein family containing a subset of 3-deoxy-D-*arabino*-heptulosonate 7-phosphate synthases. *J. Bacteriol. 180*, 119−127.

(5) Birck, M. R., and Woodard, R. W. (2001) *Aquifex aeolicus* 3-deoxy-D-*manno*-2-octulosonic acid 8-phosphate synthase: A new class of KDO 8-P synthase? *J. Mol. Evol. 52*, 205−214.

(6) Schofield, L. R., Anderson, B. F., Patchett, M. L., Norris, G. E., Jameson, G. B., and Parker, E. J. (2005) Substrate ambiguity and structure of *Pyrococcus furiosus* 3-deoxy-D-*arabino*-heptulosonate 7-phosphate synthase: An ancestral 3-deoxy-D-ald-2-ulosonate phosphate synthase? *Biochemistry 44*, 11950−11962.

(7) Cochrane, F. C., Cookson, T. V. M., Jameson, G. B., and Parker, E. J. (2009) Reversing evolution: Re-establishing obligate metal ion dependence in a metal-independent KDO8P synthase. *J. Mol. Biol. 390*, 646−661.

(8) Wang, J., Duewel, H. S., Woodard, R. W., and Gatti, D. L. (2001) Structures of *Aquifex aeolicus* KDO8P synthase in complex with R5P and PEP, and with a bisubstrate inhibitor: Role of active site water in catalysis. *Biochemistry 40*, 15676−15683.

(9) Duewel, H. S., Radaev, S., Wang, J., Woodard, R. W., and Gatti, D. L. (2001) Substrate and metal complexes of 3-deoxy-D-*manno*-octulosonate-8-phosphate synthase from *Aquifex aeolicus* at 1.9 Å resolution. Implications for the condensation mechanism. *J. Biol. Chem. 276*, 8393−8402.

(10) Shumilin, I. A., Bauerle, R., Wu, J., Woodard, R. W., and Kretsinger, R. H. (2004) Crystal structure of the reaction complex of 3-deoxy-D-*arabino*-heptulosonate-7-phosphate synthase from *Thermotoga maritima* refines the catalytic mechanism and indicates a new mechanism of allosteric regulation. *J. Mol. Biol. 341*, 455−466.

(11) Asojo, O., Friedman, J., Adir, N., Belakhov, V., Shoham, Y., and Baasov, T. (2001) Crystal structures of KDOP synthase in its binary complexes with the substrate phosphoenolpyruvate and with a mechanism-based inhibitor. *Biochemistry 40*, 6326−6334.

(12) Ahn, M., Pietersma, A. L., Schofield, L. R., and Parker, E. J. (2005) Mechanistic divergence of two closely related aldol-like enzyme-catalysed reactions. *Org. Biomol. Chem. 3*, 4046−4049.

(13) Kona, F., Xu, X., Martin, P., Kuzmic, P., and Gatti, D. L. (2007) Structural and mechanistic changes along an engineered path from metallo to nonmetallo 3-deoxy-D-*manno*-octulosonate 8-phosphate synthases. *Biochemistry 46*, 4532−4544.

(14) Duewel, H. S., and Woodard, R. W. (2000) A metal bridge between two enzyme families. 3-Deoxy-D-*manno*-octulosonate-8-phosphate synthase from *Aquifex aeolicus* requires a divalent metal for activity. *J. Biol. Chem. 275*, 22824−22831.

(15) Shulami, S., Furdui, C., Adir, N., Shoham, Y., S., A. K., and Baasov, T. (2004) A reciprocal single mutation affects the metal requirement of 3-deoxy-D-*manno*-2-octulosonate-8-phosphate

(KDO8P) synthases from *Aquifex pyrophilus* and *Escherichia coli*. *J. Biol. Chem. 279*, 45110−45120.
(16) Oliynyk, Z., Briseno-Roa, L., Janowitz, T., Sondergeld, P., and Fersht, A. R. (2004) Designing a metal-binding site in the scaffold of *Escherichia coli* KDO8PS. *Protein Eng., Des. Sel. 17*, 383−390.
(17) Li, J., Wu, J., Fleischhacker, A. S., and Woodard, R. W. (2004) Conversion of *Aquifex aeolicus* 3-deoxy-D-*manno*-octulosonate 8-phosphate synthase, a metalloenzyme, into a nonmetalloenzyme. *J. Am. Chem. Soc. 126*, 7448−7449.
(18) Shumilin, I. A., Kretsinger, R. H., and Bauerle, R. H. (1999) Crystal structure of phenylalanine-regulated 3-deoxy-D-*arabino*-heptulosonate-7-phosphate synthase from *Escherichia coli*. *Structure (Cambridge, MA, U.S.) 7*, 865−875.
(19) Kona, F., Tao, P., Martin, P., Xu, X., and Gatti, D. L. (2009) Electronic structure of the metal center in the Cd^{2+}, Zn^{2+}, and Cu^{2+} substituted forms of KDO8P synthase: Implications for catalysis. *Biochemistry 48*, 3610−3630.
(20) Allison, T. M., Hutton, R. D., Cochrane, F. C., Yeoman, J. A., Jameson, G. B., and Parker, E. J. (2011) Targeting the role of a key conserved motif for substrate selection and catalysis by 3-deoxy-D-*manno*-octulosonate 8-phosphate synthase. *Biochemistry 50*, 3686−3695.
(21) Ahn, M., Cochrane, F. C., Patchett, M. L., and Parker, E. J. (2008) Arabinose 5-phosphate analogues as mechanistic probes for *Neisseria meningitidis* 3-deoxy-D-*manno*-octulosonate 8-phosphate synthase. *Bioorg. Med. Chem. 16*, 9830−9836.
(22) Xu, X., Kona, F., Wang, J., Lu, J., Stemmler, T., and Gatti, D. L. (2005) The catalytic and conformational cycle of *Aquifex aeolicus* KDO8P synthase: Role of the L7 loop. *Biochemistry 44*, 12434−12444.
(23) Howe, D. L., Sundaram, A. K., Wu, J., Gatti, D. L., and Woodard, R. W. (2003) Mechanistic insight into 3-deoxy-D-*manno*-octulosonate-8-phosphate synthase and 3-deoxy-D-*arabino*-heptulosonate-7-phosphate synthase utilizing phosphorylated monosaccharide analogues. *Biochemistry 42*, 4843−4854.
(24) Allison, T. M., Yeoman, J. A., Hutton, R. D., Cochrane, F. C., Jameson, G. B., and Parker, E. J. (2010) Specificity and mutational analysis of the metal-dependent 3-deoxy-D-*manno*-octulosonate 8-phosphate synthase from *Acidithiobacillus ferrooxidans*. *Biochim. Biophys. Acta 1804*, 1526−1536.
(25) Ray, P. H. (1980) Purification and characterization of 3-deoxy-D-*manno*-octulosonate 8-phosphate synthetase from *Escherichia coli*. *J. Bacteriol. 141*, 635−644.
(26) Pflugrath, J. W. (1999) The finer things in X-ray diffraction data collection. *Acta Crystallogr. D55*, 1718−1725.
(27) Bailey, S. (1994) The CCP4 suite: Programs for protein crystallography. *Acta Crystallogr. D50*, 760−763.
(28) McPhillips, T. M., McPhillips, S. E., Chiu, H. J., Cohen, A. E., Deacon, A. M., Ellis, P. J., Garman, E., Gonzalez, A., Sauter, N. K., Phizackerley, R. P., Soltis, S. M., and Kuhn, P. (2002) Blu-Ice and the distributed control system: Software for data acquisition and instrument control at macromolecular crystallography beamlines. *J. Synchrotron Radiat. 9*, 401−406.
(29) McCoy, A. J., Grosse-Kunstleve, R. W., Adams, P. D., Winn, M. D., Storoni, L. C., and Read, R. J. (2007) Phaser crystallographic software. *J. Appl. Crystallogr. 40*, 658−674.
(30) Murshudov, G. N., Vagin, A. A., and Dodson, E. J. (1997) Refinement of macromolecular structures by the maximum-likelihood method. *Acta Crystallogr. D53*, 240−255.
(31) Emsley, P., and Cowtan, K. (2004) Coot: Model-building tools for molecular graphics. *Acta Crystallogr. D60*, 2126−2132.
(32) *Prime*, version 3.0 (2011) Schrodinger, LLC, New York.
(33) *Maestro*, version 9.2 (2011) Schrodinger, LLC, New York.
(34) *MacroModel*, version 9.9 (2011) Schrodinger, LLC, New York.
(35) Schrodinger Suite 2011 Induced Fit Docking protocol. *Glide*, version 5.7 (2011) Schrodinger, LLC, New York. *Prime*, version 3.0 (2011) Schrodinger, LLC, New York.
(36) Sherman, W., Day, T., Jacobson, M. P., Friesner, R. A., and Farid, R. (2006) Novel procedure for modeling ligand/receptor induced fit effects. *J. Med. Chem. 49*, 534−553.
(37) Sherman, W., Beard, H. S., and Farid, R. (2006) Use of an induced fit receptor structure in virtual screening. *Chem. Biol. Drug Des. 67*, 83−84.
(38) Li, Z., Sau, A. K., Shen, S., Whitehouse, C., Baasov, T., and Anderson, K. S. (2003) A snapshot of enzyme catalysis using electrospray ionization mass spectrometry. *J. Am. Chem. Soc. 125*, 9938−9939.